Application of a Stability-constrained Optimal Power Flow to Tuning of Oscillation Controls in Competitive Electricity Markets

Sameh K. M. Kodsi, Claudio A. Cañizares, *Fellow, IEEE*

***Abstract*— A novel technique based on a stability-constrained Optimum Power Flow (OPF) algorithm that properly captures important rotor angle and voltage stability conditions is proposed and described. The application of this technique to the optimal tuning of both Power System Stabilizers (PSS) and Thyristor Controlled Series Compensators (TCSC) to damp power system oscillations within the context of competitive electricity markets is proposed and discussed as well. The proposed technique is tested on the IEEE 14-bus benchmark system and compared with a "standard" OPF algorithm. The results obtained demonstrate the advantages of the proposed technique over existent dispatching techniques from the point of view of power dispatch and system stability conditions, and especially locational marginal prices.**

***Index Terms*— Electricity markets, locational marginal prices, optimal power flow, power system stabilizer, FACTS, tuning, voltage stability, angle stability, power system oscillations.**

I. Introduction

THE operation of power systems has been significantly affected by the deregulation process. Nowadays, increased load demand and the need to operate the system based mainly on economic considerations have led to many concerns regarding the secure operation of power systems. In this environment, Independent System Operators (ISOs) are in charge of guaranteeing stable, secure and reliable operation of the power grid, which includes proper tuning of the different available controllers to enhance system security. Hence, there is a need for tuning techniques that guarantee system stability within the context of a market operating environment. This paper tries to address some of these issues by focusing on a better representation of oscillatory and voltage instabilities within current market clearing and dispatch mechanisms.

Various algorithms have been proposed to include stability constraints in the OPF. In [1] and [2], the authors propose the use of the minimum singular value of the power flow Jacobian as an index to detect proximity to voltage instability, which is then used as a stability constraint to develop a voltage-stability-constrained OPF (VSC-OPF) in [3]. In [4], a different strategy is proposed based on the use of a multi-objective OPF technique to maximize both social benefit and the distance to a voltage instability point. The problem with the inclusion of voltage security constraints alone is that, in some power systems, oscillatory instabilities (inter-area or plant oscillation modes) are one of the limiting factors in maintaining system security [5] (e.g. WSCC, now WECC, August 96 blackout). In [6], a stability-constrained OPF is proposed, considering some of the generator dynamic equations, but it does not account for other important variables in stability studies such as voltage regulators. The technique discussed in [7] addresses some of these shortcomings by using a stability index proposed in [5] to develop a small-perturbation-stability-constrained OPF (SSC-OPF), which considers both voltage and oscillatory instabilities using detailed dynamic models. Although this technique offers a new methodology for pricing of the dynamic services provided by Power System Stabilizers (PSS) or other controllers such as FACTS, these controllers should be first tuned to "optimize" market operating conditions, i.e. power dispatch and price levels, as well as guaranteeing an adequate level of system security. Thus, the current paper discusses the use of the SSC-OPF for optimally tuning these controllers within the context of an electricity market clearing mechanism, comparing it against a more "classical" approach based on the resulting market and system operating conditions.

The tuning of PSS and TCSC is discussed in [8], [9], concentrating on better coordination to enhance oscillation damping by using an optimization-based tuning algorithm. In [10], the optimal tuning of PSS and FACTS controllers is accomplished using a simple parameter-constrained nonlinear optimization algorithm to minimize an implicit objective function that accounts for oscillatory instabilities. Another approach is presented in [11], [12] by formulating an eigenvalue-based objective function to insure system damping enhancement during the tuning process. Similarly, in [13], the authors discuss PSS design based on a multi-objective optimization algorithm to enhance system damping. All these approaches concentrate on system damping enhancement and the effect of the interaction between PSS and TCSC on the oscillatory instability. The effect of controller tuning on market and system operating conditions within the context of deregulated operating environments is somewhat dealt with in [14], where the effect of PSS on power system stability is priced based on game theory; besides this work, there is very little research reported in the literature on this particular issue. Thus, the present paper concentrates on discussing the effect of the tuning process of system controllers on the operation of electricity markets and their associated power systems,

Accepted for publication March 2007.

This work was supported by the National Science and Engineering Research Council (NSERC) of Canada.

S. Kodsi is with AMEC Americas, 2020 Winston Park Drive, Suite 700, Oakville, ON, L6H 6X7, Canada. Email: sameh.kodsi@amec.com

C. Cañizares is with the Department of Electrical and Computer Engineering, University of Waterloo, Waterloo, ON, N2L 3G1, Canada. Email: ccanizar@uwaterloo.ca

using a novel SSC-OPF algorithm that better represents system security.

It is important to highlight the fact that the current paper concentrates on discussing a particular application of a novel SSC-OPF technique, utilizing a better representation of system dynamics on the proposed optimization model to study the effect of controller tuning on the electric system and market conditions, particularly LMPs. This is only a part of what would be required to properly manage and price system stability and security in competitive electricity markets, given the technical and economic complexities associated with these issues, which lead to decouple some of the ancillary service markets that are used to purchase the services required to ensure proper security margins from energy markets. For example, in [15], a decoupled reactive power market model is proposed and discussed in detail, and in [16], the authors propose a generic model of an ancillary service market that would run concurrently with the energy market.

The paper is organized as follow: Section II discusses the basic concepts of a standard-OPF-based market auction mechanism, and presents a novel SSC-OPF-based market clearing technique on which the proposed optimal tuning method is based. In Section III, the application of the SSC-OPF is illustrated using the IEEE 14-bus benchmark system, and the results are compared with the results obtained from a standard market clearing mechanism. The inclusion of PSS and TCSC controllers to enhance the overall stability of the test system, and the use of the SSC-OPF for the optimal tuning of the controllers' gain are discussed in Section IV. Finally, Section V discusses the main contributions of this paper and possible future research directions.

II. Background Review

A. Standard OPF Auction

The OPF-based auction is basically defined as a non-linear constrained optimization problem, and consists of a scalar objective function (S_b), and a set of equality and inequality constraints. The following optimization problem represents a typical OPF-based auction model [4], [17]:

$$\begin{aligned} \text{Min.} \quad & S_b(x,p,\lambda) = -(C_d^T P_d - C_s^T P_s) \\ \text{s.t.} \quad & F_{PF}(\delta, V, Q_G, P_s, P_d) = 0 \\ & 0 \le P_s \le P_{s_{\max}} \\ & 0 \le P_d \le P_{d_{\max}} \\ & \mid P_{ij}(\delta, V) \mid \le P_{ij_{\max}} \\ & I_{ij}(\delta, V) \le I_{ij_{\max}} \\ & Q_{G_{\min}} \le Q_G \le Q_{G_{\max}} \\ & V_{\min} \le V \le V_{\max} \end{aligned} \tag{1}$$

where C_s and C_d are vectors of supply and demand bids in \$/MWh, respectively; P_s and P_d are the supply and demand power bids respectively, which can not exceed their maximum values; $F_{PF}(\cdot)$ represent the "classical" power flow equations; Q_G stands for the generator reactive powers; V and δ define the bus phasor voltages; P_{ij} stand for the power flowing through the lines, which are used to represent system security by imposing limits on them, in addition to line current I_{ij} thermal limits and bus voltage limits. In this model, which is typically referred to as a security-constrained OPF-based auction, P_{ij} limits are typically obtained by means of off-line angle and/or voltage stability studies [18]. These limits do not present the actual stability conditions of the resulting solutions, since these are not the actual operating conditions corresponding to the solution of the OPF-based auction. Hence, this model may lead in some cases to insecure solutions and/or inappropriate price signals, as demonstrated here.

B. Small-Perturbation-Stability Constrained OPF [7]

In general, power system stability problems can be classified into three main categories, namely, angle, frequency, and voltage stability problems [19]. Stability problems may result from large or small disturbances. For example, first swing stability problems occur due to large disturbances in the system; these problems can be monitored using time domain simulation tools. Oscillatory instabilities and voltage collapse problems, on the other hand, may be associated with large or small disturbances; these phenomena are usually studied using steady state analysis tools. Thus, voltage stability problems are typically associated with saddle-node or limit induced bifurcations, which lead to voltage collapse [20]. Lack of sufficient damping torque leads to oscillatory instabilities, which may be associated with Hopf bifurcations (e.g. [5], [21]).

Based on the equations of the various components and their control models, the power system modeling used in this paper is represented by the following set of differential and algebraic equations (DAE) [22]:

$$\begin{bmatrix} \dot{x} \\ 0 \end{bmatrix} = \begin{bmatrix} f(x,y,p) \\ g(x,y,p) \end{bmatrix} = F(x,y,p) \tag{2}$$

where:

- $x = [\delta_G^T\ \omega^T\ {E'_q}^T\ {E'_d}^T\ E_{fd}^T\ V_R^T\ R_f^T\ x_{cont}^T]^T \in \Re^n$ is a vector of state variables that represents the dynamic states of generators, loads, and other system controllers. Thus, δ_G represents the generator torque angles; ω stands for the rotor speed variations; E'_q stands for the quadrature components of the generator internal voltages; E'_d represents the direct components of the generator internal voltages; E_{fd} stands for the exciter output voltages; V_R represents the voltage regulator output voltages; R_f stands for the rate of feed-back of the exciter output voltages; and x_{cont} represents all the dynamic variables of PSS and FACTS controllers, such as the PSS voltage signal or the TCSC controlled variable reactance.
- $y = [\delta^T\ V^T\ Q_G^T]^T \in \Re^m$ is a vector of steady-state algebraic variables that typically result from neglecting fast dynamics (e.g. load voltage phasor magnitudes and angles). Thus, δ stands for the bus voltage phasor angles; V represents the bus voltage phasor magnitudes; and Q_G stands for the bus generated reactive powers.
- $p = [P_G^T\ P_L^T\ Q_L^T\ V_{oG}^T\ P_{oTCSC}^T K]^T \in \Re^k$ is a set of the controllable and uncontrollable parameters such as Automatic Voltage Regulator (AVR) settings or load levels. Thus, P_G represents the total generator power; P_L and Q_L stand for active and reactive power total demand,

respectively; V_{o_G} represents the reference voltage settings of the generators; $P_{o_{TCSC}}$ represents the active power settings of the TCSC; and K stands for the PSS and TCSC controller PI gains.

- The vector field $f(\cdot) = [f_G^T(\cdot)\ f_{AVR}^T(\cdot)\ f_{cont}^T(\cdot)]^T : \Re^n \times \Re^m \times \Re^k \mapsto \Re^n$ stands for the system non-linear differential (state) equations [22]. Thus, $f_G(\cdot)$ stands for the generator state equations (generator 4^{th} order transient model); $f_{AVR}(\cdot)$ represent the voltage regulator state equations (IEEE Type 1); and $f_{cont}(\cdot)$ stands for the state equations of the PSS and TCSC.
- The vector field $g(\cdot) = [g_G^T(\cdot)\ g_L^T(\cdot)]^T : \Re^n \times \Re^m \times \Re^k \mapsto \Re^m$ represents the system algebraic constraints [22]. Thus, $g_G(\cdot)$ stands for the generators' stator algebraic equations, and $g_L(\cdot)$ represents the power flow equations of the transmission network.
- $F(\cdot) = [f^T(\cdot)\ g^T(\cdot)]^T$.

In small-perturbation stability analysis, (2) is linearized around an equilibrium or operating point (x_o, y_o) for given values of the parameters p_o. Thus,

$$\begin{bmatrix} \Delta\dot{x} \\ 0 \end{bmatrix} = \underbrace{\begin{bmatrix} J_1 & J_2 \\ J_3 & J_4 \end{bmatrix}}_{J} \begin{bmatrix} \Delta x \\ \Delta y \end{bmatrix} \tag{3}$$

where, J is the system Jacobian, i.e. $J_1 = \partial f/\partial x|_0$, $J_2 = \partial f/\partial y|_0$, $J_3 = \partial g/\partial x|_0$, $J_4 = \partial g/\partial y|_0$. Thus, a complex pair of eigenvalues of J can be represented as:

$$\begin{bmatrix} J_1 & J_2 \\ J_3 & J_4 \end{bmatrix} \begin{bmatrix} v_{1_R} \pm jv_{1_I} \\ v_{2_R} \pm jv_{2_I} \end{bmatrix} = [\alpha \pm j\beta] \begin{bmatrix} v_{1_R} \pm jv_{1_I} \\ 0 \end{bmatrix} \tag{4}$$

By separating the real and imaginary parts and rearranging these equations, one has:

$$\left(\underbrace{\begin{bmatrix} J & \beta B \\ -\beta B & J \end{bmatrix}}_{J_m} - \alpha \begin{bmatrix} B & 0 \\ 0 & B \end{bmatrix} \right) \begin{bmatrix} v_{1_R} \\ v_{2_R} \\ v_{1_I} \\ v_{2_I} \end{bmatrix} = 0 \tag{5}$$

where $B = \begin{bmatrix} I & 0 \\ 0 & 0 \end{bmatrix}$. Since at a Hopf bifurcation $\alpha = 0$, the matrix J_m becomes singular, and the same holds at a saddle-node bifurcation point where $\alpha = \beta = 0$. Therefore, the minimum singular value of the modified full Jacobian matrix J_m can be used as an index to indicate proximity to a Hopf or a saddle-node bifurcation. Consequently, the following stability index is proposed in [5]:

$$HBI = \sigma_{min}(J_m) \tag{6}$$

This index is shown in [5] to have a fairly linear behavior with respect to changes on system loading, with no significant discontinuities due to control limits for a series of practical examples; this particular behavior is also observed in the current paper for the test system used (see Section IV). Nevertheless, even in the presence of possible discontinuities, these would not be a significant factor for the proposed SSC-OPF technique, where this index is used as a security constraint as explained below; this is due to the fact that one is only concerned about the value of this index "near" a bifurcation point, where it can be formally demonstrated that the index is smooth and quasi-linear [5], [23], given that it is only at this point where this security constraint becomes binding.

Therefore, the following OPF-based auction [7], which includes this index as a constraint, is proposed here as a better alternative to properly represent these types of stability problems:

$$\begin{aligned} \text{Min.} \quad & S_b = -(C_d^T P_d - C_s^T P_s) \\ \text{s.t.} \quad & F(x, y, p) = 0 \\ & \sigma_{min}(J_m) \geq \ \sigma_c \\ & p_{min} \leq p \leq p_{\max} \\ & I_{ij}(x, y) \leq I_{ij_{\max}} \\ & y_{\min} \leq y \leq y_{\max} \end{aligned} \tag{7}$$

where x, y, p and $F(\cdot)$ are defined in (2); σ_{min} is the minimum singular value of the modified state matrix J_m, which becomes zero at a Hopf or saddle-node bifurcation point; σ_c stands for the minimum stability index value as defined by the user; and P_d and P_s are contained in P_L and P_G in p, respectively. The value of σ_c depends on the system characteristics, and thus has to be determined based on off-line stability studies, so that it reflects appropriate system security margins (e.g. appropriate damping ratios) under an N-1 contingency criterion. This particular issue is discussed in more detail in Section III.

C. Solution Procedure

The SSC-OPF (7) is basically a nonlinear optimization problem, with an implicit constraint; hence, "standard" optimization solution techniques must be modified to be able to solve this problem. In this paper, an Interior Point method is used as the base to solve the proposed optimization problem. Thus, from (7), the OPF auction can be rewritten in the following form:

$$\begin{aligned} \text{Min.} \quad & S(\chi) \\ \text{s.t.} \quad & F(\chi) = 0, \\ & \underline{H} \leq H(\chi) \leq \overline{H}, \end{aligned} \tag{8}$$

where $\chi \in \Re^N$ is the vector of the optimization variables i.e. $\chi = [x^T \quad y^T \quad p^T]^T$, and $N = n + m + k$, with lower bounds $\underline{\chi}$ and upper bounds $\overline{\chi}$; $S : \Re^N \rightarrow \Re$ is the scalar optimization function; $F : \Re^N \rightarrow \Re^{n+m}$ is the vector function defined in (2); and $H : \Re^N \rightarrow \Re^l$ is a vector function, with lower bounds $\underline{H}$ and upper bounds $\overline{H}$, used to represent all operating limits of the system, including limits in χ and the stability constraint represented by the $\sigma_{min}(J_m)$ index. This optimization problem is solved here using an Interior Point method, which first transforms all inequality constraints in (8) into equalities by adding non-negative slack vectors s and q, and thus incorporates them into logarithmic barrier terms as follows [24], [25]:

$$\begin{aligned} \text{Min.} \quad & S(\chi) - \mu_s \sum_i (\ln s_i + \ln q_i) \\ \text{s.t.} \quad & F(\chi) = 0, \\ & -s - q + \overline{H} - \underline{H} = 0, \\ & -H(\chi) - q + \overline{H} = 0, \\ & s \geq 0, \quad q \geq 0 \end{aligned} \tag{9}$$

where $\mu_s \in \Re$, $\mu_s > 0$, is the barrier parameter. To solve the equality-constrained problem (9), the Lagrange-Newton method is used. Thus, the Lagrangian function $L_\mu(u)$ associated with (9) is given by:

$$L_\mu(u) = S(\chi) - \mu_s \sum_i (\ln s_i + \ln q_i) - \rho^T F(\chi) - \varsigma^T(-s - q + \overline{H} - \underline{H}) - \tau^T(-H(\chi) - q + \overline{H}) \quad (10)$$

where $\rho \in \Re^{n+m}$, $\varsigma \in \Re^l$, and $\tau \in \Re^l$ are vectors of Lagrange multipliers, or dual variables, and $u = [\chi^T \;\; s^T \;\; q^T \;\; \rho^T \;\; \varsigma^T \;\; \tau^T]^T$. A local minimum of (10) is expressed in terms of a stationary point of $L_\mu(u)$, which must satisfy the Karush-Kuhn-Tucker (KKT) optimality conditions $\nabla_u L_\mu(u) = 0$. Although this system is nonlinear, its solution is usually approximated by a single iteration of Newton's method; hence, the Hessian $\nabla^2_\chi L_\mu(u)$ is required in the algorithm. The computation of this Hessian requires the evaluation of the objective function Hessian $\nabla^2_\chi S(\chi)$ and the constraint Hessians $\nabla^2_\chi F(\chi)$ and $\nabla^2_\chi H(\chi)$, since:

$$\nabla^2_\chi L_\mu(u) = \nabla^2_\chi S(\chi) - \rho^T \nabla^2_\chi F(\chi) + \tau^T \nabla^2_\chi H(\chi) \quad (11)$$

To obtain a solution to this problem, a good estimate of $\nabla^2_\chi \sigma_{min}(J_m)$ is needed. This requires certain approximations, since $\sigma_{min}(J_m)$ is an implicit function of the optimization variables χ, which is accomplished here by first obtaining an estimate of $\nabla_\chi \sigma_{min}(J_m)$, based on [1]. Thus, if χ_* is perturbed such that $\chi_* + \Delta\chi = [z_*^T + \Delta z^T \;\; p_*^T + \Delta p^T]^T$, where $z = [x^T \;\; y^T]^T$, using a Taylor series expansion:

$$J|_{z_*+\Delta z} \approx J|_{z_*} + G\Delta z \quad (12)$$

where $G = \left.\frac{\partial^2 F}{\partial z^2}\right|_{z_*}$. Hence, from (5)

$$J_m|_{z_*+\Delta z} \approx \begin{bmatrix} J|_{z_*+\Delta z} & \beta|_{z_*+\Delta z} B \\ -\beta|_{z_*+\Delta z} B & J|_{z_*+\Delta z} \end{bmatrix} \approx \begin{bmatrix} J|_{z_*} + G\Delta z & \beta B \\ -\beta B & J|_{z_*} + G\Delta z \end{bmatrix} \quad (13)$$

assuming that $\beta|_{z_*+\Delta z} \approx \beta|_{z_*} \approx \beta$, i.e. the frequency of the critical eigenvalues (the eigenvalues that eventually reach the imaginary axis for a saddle-node or Hopf bifurcation) does not change significantly, which is typically the case [5]. Then,

$$J_m|_{z_*+\Delta z} \approx J_m|_{z_*} + \begin{bmatrix} G\Delta z & 0 \\ 0 & G\Delta z \end{bmatrix} \quad (14)$$

Following [1], and based on (14), one can then approximate the changes on $\sigma_{min}(J_m)$ using the following formula:

$$\Delta\sigma_{min}(J_m) \approx U_1^T \begin{bmatrix} G\Delta z & 0 \\ 0 & G\Delta z \end{bmatrix} V_1 \quad (15)$$

where U_1 and V_1 are respectively the left and right singular vectors corresponding to the minimum singular value of J_m. Furthermore, since at a solution point χ_*:

$$F(\chi_*) = F(z_*, p_*) = 0$$
$$\left.\frac{\partial F}{\partial z}\right|_{z_*} dz + \left.\frac{\partial F}{\partial p}\right|_{p_*} dp = 0$$
$$\Rightarrow \Delta z = -\left[\left.\frac{\partial F}{\partial z}\right|_{z_*}\right]^{-1} \left.\frac{\partial F}{\partial p}\right|_{p_*} \Delta p = -J^{-1} J_p \Delta p \quad (16)$$

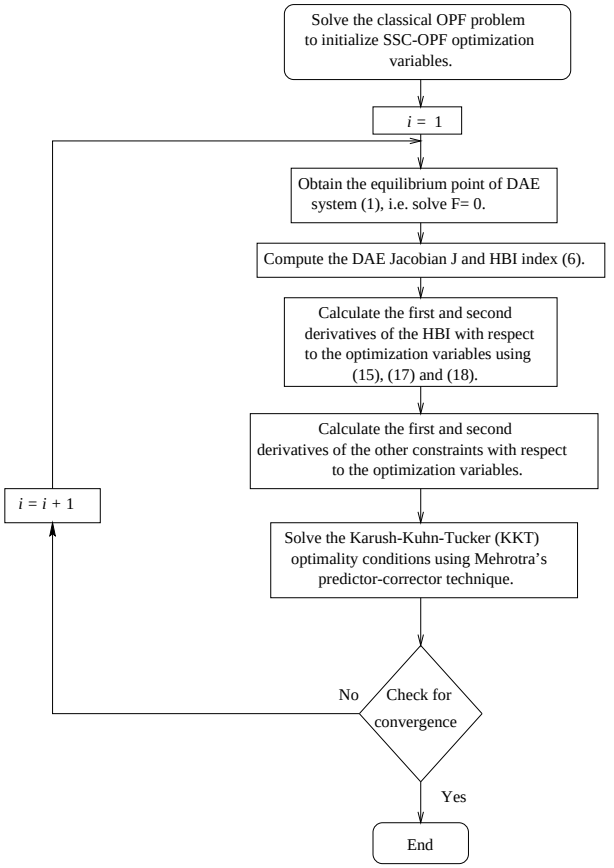

Fig. 1. SSC-OPF solution procedure.

one can evaluate the change of $\sigma_{min}(J_m)$ with respect to the parameters p as follows:

$$\Delta\sigma_{min}(J_m) \approx U_1^T \begin{bmatrix} -GJ^{-1}J_p\Delta p & 0 \\ 0 & -GJ^{-1}J_p\Delta p \end{bmatrix} V_1 \quad (17)$$

Thus, to evaluate $\nabla^2_\chi \sigma_{min}(J_m)$, the following numerical approximation is used [26]:

$$\left.\frac{\partial^2 \sigma_{min}(J_m)}{\partial\chi_i\chi_j}\right|_{\chi_*+\Delta\chi} \approx \frac{\left.\frac{\partial\sigma_{min}(J_m)}{\partial\chi_i}\right|_{\chi_*} - \left.\frac{\partial\sigma_{min}(J_m)}{\partial\chi_i}\right|_{\chi_*+\Delta\chi}}{\Delta\chi_j} \quad (18)$$

where the $\frac{\partial\sigma_{min}}{\partial\chi_i}$ are obtained using the approximations (15) or (17) as needed.

D. Implementation of SSC-OPF

Figure 1 depicts the computational procedure used to solve the proposed SSC-OPF using a primal-dual-IP method based on a Mehrotra's predictor-corrector technique programmed in MATLAB [25]. Observe that the equilibrium equations of the dynamic DAE model as well as their corresponding Jacobian and eigenvalues closer to the imaginary axis are computed at every iteration i. This procedure can be summarized as follows:

1) The proposed SSC-OPF is initialized using the results obtained from applying the standard OPF (1) to the system.
2) The equilibrium equations of (2), i.e. $F(\cdot) = 0$, are solved.

3) The first and the second derivatives of the equality and inequality constraints are calculated, including the first and second derivatives of the stability constraint with respect to the optimization variables using (15), (17) and (18).
4) The Karush-Kuhn-Tucker (KKT) optimality conditions are then formulated and solved using Mehrotra's predictor-corrector technique, and the barrier parameter μ_s is updated using the techniques described in [24], [25].
5) If the barrier parameter, the objective function and the optimization variables converge within the given tolerance limits (10^{-4}), the process stops, otherwise it is repeated from Step 2.

To evaluate the computational burden of the proposed SSC-OPF technique, the CPU times for the standard OPF (1) and the SSC-OPF (7) were compared for the test system discussed in Section III. It took about 5 to 20 CPU minutes to obtain a SSC-OPF solution, depending on the loading level, with CPU times increasing as the system was more loaded and hence closer to the σ_c value in (7). The standard OPF required in general about 5% of the CPU time needed by the SSC-OPF to obtain a solution, while both need about 40 to 50 iterations to converge to an optimal solution. The application of the proposed technique to the more realistic 50-machine, 145-bus IEEE benchmark system described in [27] resulted in CPU times of a few minutes to a few hours to obtain solutions at different loading conditions. Even though these CPU times may be significantly reduced by optimizing the code (e.g. using sparse matrix techniques), additional computational costs are to be expected, since the number of constraints and the sizes of the associated Jacobians and Hessians is larger in the proposed SSC-OPF method that in the standard OPF, and the linearization of the required derivatives of σ_{min} certainly affect the convergence characteristics. Hence, until more efficient and robust numerical techniques are developed to solve the optimization model with implicit constraint (7), the proposed methodology seems more suitable for off-line types of applications, such as the optimal tuning application proposed and discussed in Section IV.

E. Locational Marginal Prices

OPF-based market models produce the optimal operating point and a variety of sensitivities through the Lagrangian multipliers. These multipliers are associated with the Locational Marginal Prices (LMPs) at each node [4], which can provide reliable pricing indicators [17]. The Lagrangian multipliers of the power flow equations, which are a subset of ρ in (10), are used to define the LMPs for all participants in the auction as follows:

$$\begin{aligned} \frac{\partial L_\mu(z)}{\partial P_{s_j}} &= C_{s_j} - \rho_{P_{s_j}} + \varsigma_{P_{s_{max_j}}} \\ &\quad + \tau_{\sigma_{min}} \left(\frac{\partial \sigma_{min}(J_m)}{\partial P_{s_j}} \right) = 0 \\ \frac{\partial L_\mu(z)}{\partial P_{d_j}} &= -C_{d_j} + \rho_{P_{d_j}} + \varsigma_{P_{d_{max_j}}} \end{aligned} \tag{19}$$

TABLE I
GENCOs AND ESCOs BIDDING DATA

	$P_{d_{max}}$ or $P_{s_{max}}$ (MW)	C_d or C_s ($/MWh)
GENCO1	615	9.50
GENCO2	60	10.20
GENCO3	60	11.30
ESCO2	30.38	13.00
ESCO3	131.9	13.20
ESCO4	66.92	12.10
ESCO5	10.64	12.33
ESCO6	15.68	12.24
ESCO9	41.3	13.55
ESCO10	12.6	14.66
ESCO11	4.9	13.67
ESCO12	8.54	14.62
ESCO13	18.9	14.22
ESCO14	20.86	14.45

$$+\tau_{\sigma_{min}} \left(\frac{\partial \sigma_{min}(J_m)}{\partial P_{d_j}} \right) = 0$$

Hence, the LMPs for can be defined as follows:

$$\begin{aligned} LMP_{s_j} = \rho_{P_{s_j}} &= C_{s_j} + \varsigma_{P_{s_{max_j}}} \\ &\quad + \tau_{\sigma_{min}} \left(\frac{\partial \sigma_{min}(J_m)}{\partial P_{s_j}} \right) \\ LMP_{d_j} = \rho_{P_{d_j}} &= C_{d_j} - \varsigma_{P_{d_{max_j}}} \\ &\quad - \tau_{\sigma_{min}} \left(\frac{\partial \sigma_{min}(J_m)}{\partial P_{d_j}} \right) \end{aligned} \tag{20}$$

Consequently, from (20), the LMPs are affected by the costs C_s and C_d as well as the system constraints, particularly the stability constraint associated with $\sigma_{min}(J_m)$, and are a byproduct of the solution process. These LMPs can be used to analyze the effect of system constraints, such as security limits, in the market's prices, and are hence used here to evaluate the effect of the controller tuning on these market signals.

III. STANDARD OPF AND SSC-OPF AUCTION COMPARISON

In this section, the results of applying the Standard OPF-based auction (1) and the SSC-OPF auction (7) to the IEEE 14-bus test system are presented and discussed.

A single-line diagram of the IEEE 14-bus test system is shown in Fig. 2. It consists of five synchronous machines with IEEE type-1 exciters, two of which are synchronous compensators used only for reactive power support. There are 11 loads in the system totaling 259 MW and 81.3 Mvar. The static and dynamic data for the system can be found in [28], and the market bidding data is illustrated in Table I (the GENCO and ESCO numbers in this table correspond to the bus number in Fig. 2).

The selection of the test system is based on the following criteria:

1) The stability of the selected system has been modeled and analyzed, including FACTS, in detail in several technical documents based on results obtained using a variety of software packages (e.g. [28], [29]). This sample system contains enough dynamic and static elements to allow for meaningful stability and security studies.

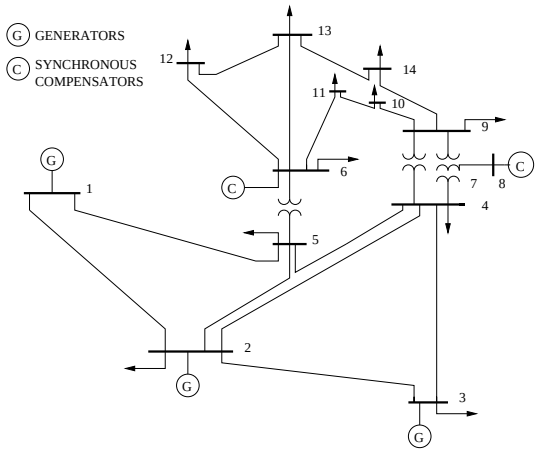

Fig. 2. IEEE 14-bus test system.

2) The selected system represents a portion of the American Power System in the US Midwest, and hence can be considered a "realistic" example.
3) The system has enough generation and load to simulate an electricity market and thus produce meaningful results that allow to analyze the proposed techniques.
4) The use of a larger system would not allow to readily analyze and thus illustrate the differences between the SSC-OPF technique and a standard OPF auction, since large number of data and computations would be required to arrive to conclusions that can also be attained with this reduced size system.

The loads in the system are typically represented in steady state as constant PQ loads with constant power factor, and are assumed to increase for the purpose of stressing the system as follows:

$$\begin{aligned} P_L &= P_{L_o} + P_d \\ P_d &\leq P_{d_{max}} = \lambda P_{L_o} \\ Q_L &= P_L \tan\phi \end{aligned} \tag{21}$$

where P_{L_o} is the "base" real and power that represents inelastic loads, ϕ stands for the constant power factor angle, and λ is a p.u. loading factor. Hence, in the standard OPF and SSC-OPF studies, the change in generated power is represented as:

$$P_G = P_{G_o} + P_s \tag{22}$$

where P_{G_o} stands for must run generation that is not included in the market bidding.

Figure 3 shows the HBI stability index (6) as the ESCOs' demand power is increased from its nominal value according to (21) with $P_d = \lambda P_{L_o}$. The HBI index is calculated assuming that the total demand is shared between GENCO1, GENCO2 and GENCO3 in proportion to their inertias, i.e. OPF techniques are not applied in this case to determine optimal schedules. This figure shows that there is a Hopf bifurcation point when the ESCOs loading factor reaches 0.45 p.u., which is associated with an oscillatory instability linked to GENCO1. On the other hand, Fig. 4 shows the HBI stability index with different contingencies applied to the system. In this case, a line 1-5 outage is determined to be the most severe

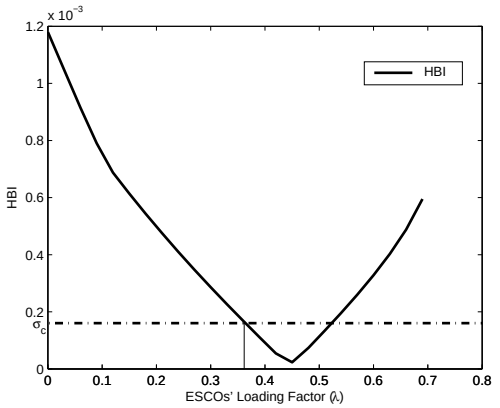

Fig. 3. HBI and minimum singular value of power flow Jacobian versus loading factor.

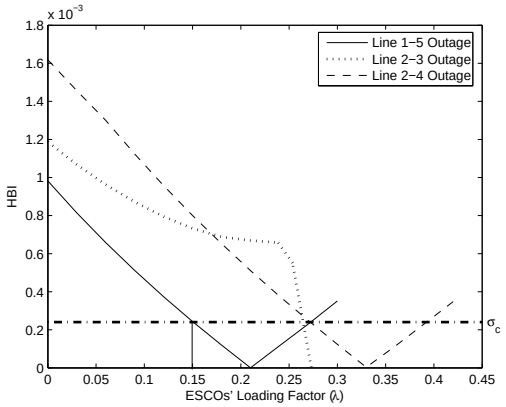

Fig. 4. HBI stability index for different contingencies applied to the system.

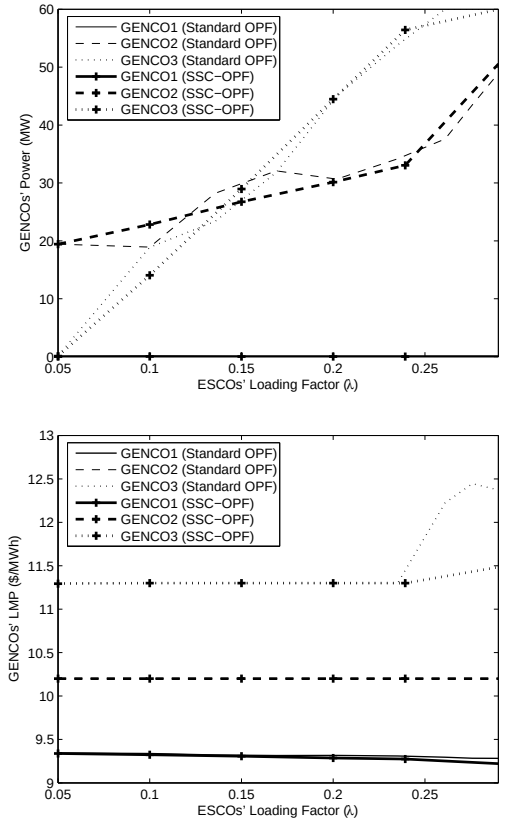

Fig. 5. GENCOs' supplied power and LMPs with respect to loading levels.

contingency from an oscillatory stability point of view, which is the main concern in this paper, and thus this outage is used to illustrate the differences between a standard OPF and the SSC-OPF under an N-1 security criterion.

Based on [30], a 2% damping ratio is used here as the minimum value of system damping required to maintain the system secure. Without contingencies, this limit is reached at an ESCOs' loading factor of 0.37 p.u., which corresponds in Fig. 3 to an HBI value of 0.00018; thus, the value of σ_c in (7) would be chosen in this case to be 0.0002. Applying an N-1 contingency criterion, the value of σ_c in (7) obtained from Fig. 4 is 0.00025.

The SSC-OPF (7) results with $\sigma_c = 0.00025$ are compared here with a standard OPF (1) results. The power limits on the lines used in (1) are obtained from eigenvalue studies and considering a damping ratio of 2% for the worst single contingency (line 1-5 outage), as typically done in most systems (e.g. Ontario). For both the standard OPF and the SSC-OPF problems, the bus voltage limits used in the optimization process are 0.9 p.u. and 1.1 p.u. The current thermal limits are set to 1.5 to 2 times the currents for the worst system contingency (N-1 contingency criterion), and hence only become an issue at high loading conditions when the system voltage stability limits are reached.

The supplied power by GENCOs and their LMPs obtained by solving (1) and (7) with respect to the ESCOs' loading factor λ are illustrated in Fig. 5. Notice that both GENCO2 and GENCO3 supply all the demand needs, while GENCO1 is not dispatched ($P_{G_1} = 0$). Furthermore, notice that the GENCOs' LMPs are higher for the standard OPF (1) than those obtained with the SSC-OPF (7), as the system is less congested in the latter case than the former due to the different security constraints used in these OPFs to represent system stability. Similar results are obtained for the ESCOs' LMPs, as shown in Fig. 6 for a selection of "remote" load buses.

These results clearly show the more restrictive nature of the "classical" security constraints used in the standard OPF, as opposed to the $\sigma_{min}(J_m)$ constraint used in the SSC-OPF. Thus, the bus prices for the standard OPF are higher than those for the SSC-OPF, in spite of both solutions being very similar from the dispatch and stability point of view, as demonstrated by the $\sigma_{min}(J_m)$ plots depicted in Fig. 7.

IV. Optimal Tuning of Oscillation Damping Controllers

The test system is analyzed in this section with the inclusion of a PSS and a TCSC. These controllers are added to the system, as shown in Fig. 8, to study their effect on system stability and LMPs using the proposed SSC-OPF technique, as this was shown to be superior to a standard OPF-based approach. The results in this section were obtained without considering system contingencies, given their rather restrictive nature, since these significantly limit the loading range for stability studies. There is no reason to expect that considering contingencies would affect the main conclusions of the analysis presented here, other than affecting the actual values, as illustrated in the previous section.

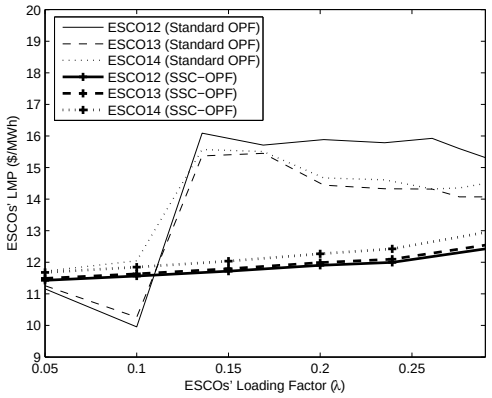

Fig. 6. Some ESCOs' LMPs with respect to loading levels.

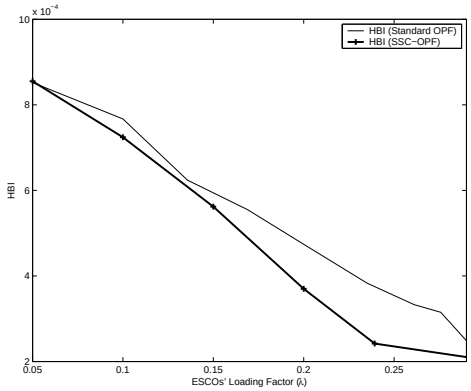

Fig. 7. HBI results obtained with the standard OPF and the SSC-OPF.

A. Optimal Tuning of PSS

A PSS can be viewed as an additional control block used to enhance the system stability [31]. This controller uses stabilizing feedback signals such as shaft speed, terminal frequency and/or power to change the input signal of the AVR. A PSS contains basically three blocks: The first block is the stabilizer Gain block with the constant gain K_{PSS}, which determines the amount of damping. The second is the Washout block, which serves as a high-pass filter, with a time constant that allows the signal associated with oscillations in rotor speed to pass unchanged, and does not allow the steady state changes to modify the terminal voltages. The last block is the Phase-compensation block, and provides the desired phase-lead characteristic to compensate for the phase lag between the AVR input and the generator electrical (air-gap) torque; in practice, two or more first-order blocks may be used to achieve the desired phase compensation.

Figure 9 shows the effect of the PSS K_{PSS} gain on the HBI as the ESCOs' demand power is increased from its nominal value according to (21) with $P_d = \lambda P_{L_o}$. The HBI index is calculated assuming again that the total demand is shared between GENCO1, GENCO2 and GENCO3 in proportion to their inertias, i.e. OPF techniques are not applied in this case to determine optimal schedules. Notice the significant effect of K_{PSS} on system stability, as expected, illustrating the need to properly choose the PSS gain that best enhances system stability. In general, as this gain is increased, the system

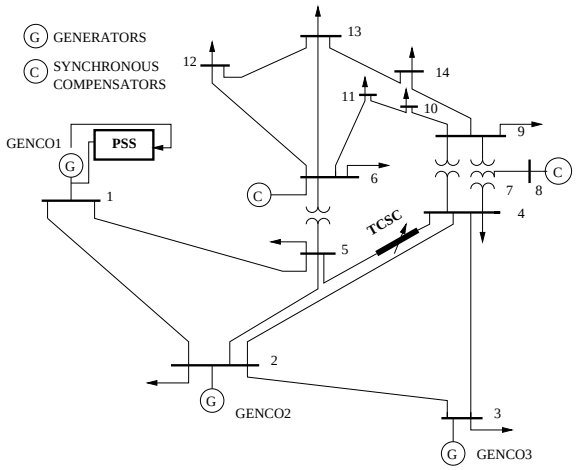

Fig. 8. IEEE 14-bus test system with PSS and TCSC.

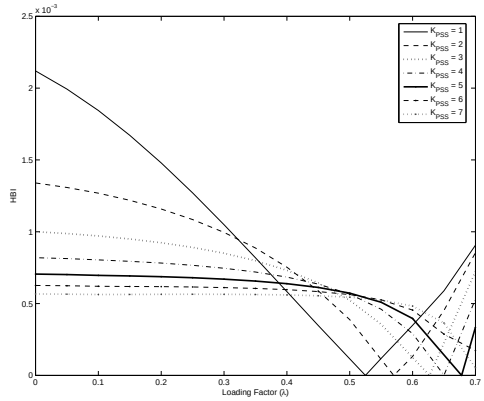

Fig. 9. Effect of the PSS gain on the HBI.

becomes more stable, with the loadability margin increasing.

Figures 10 and 11 show the results of solving the SSC-OPF problem (7) with and without optimal tuning for supply and demand, respectively. The PSS gain is chosen to be $K_{PSS} = 2.5$ for the fixed-gain studies (no tuning), as it yields a 2% damping ratio at the original Hopf bifurcation point $\lambda = 0.45$ p.u. Observe that for the optimal tuning of the PSS, the overall system and market conditions improve as the system changes due to demand increases; thus, the operating margin of the system expands beyond a loading factor of 0.5 p.u., which is the limit for the SSC-OPF with fixed K_{PSS}. The K_{PSS} optimal values obtained from the SSC-OPF with respect to load increases are illustrated in Fig. 12; these are the values used in the optimally tuned SSC-OPF solution results illustrated in Fig.10 and 11. Notice that the PSS gain increases as the demand increases, as expected from the results shown in Fig. 9.

In order to illustrate the value of the optimal tuning of the PSS gain for the market, the effect of the tuning of the PSS on the "congestion costs", i.e. $\sum_j \text{LMP}_{Lj} P_{Lj} - \text{LMP}_{Gj} P_{Gj}$, when solving the SSC-OPF problem (7) with and without tuning is depicted in Fig. 13. The results show that with the optimal tuning of the PSS gain, the system becomes less congested when the controller is properly tuned.

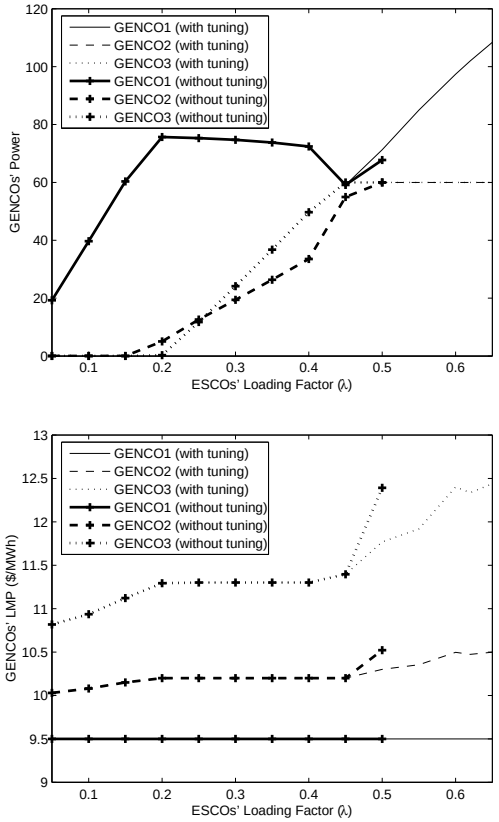

Fig. 10. GENCOs' supplied power and LMPs with respect to loading factor for system with PSS.

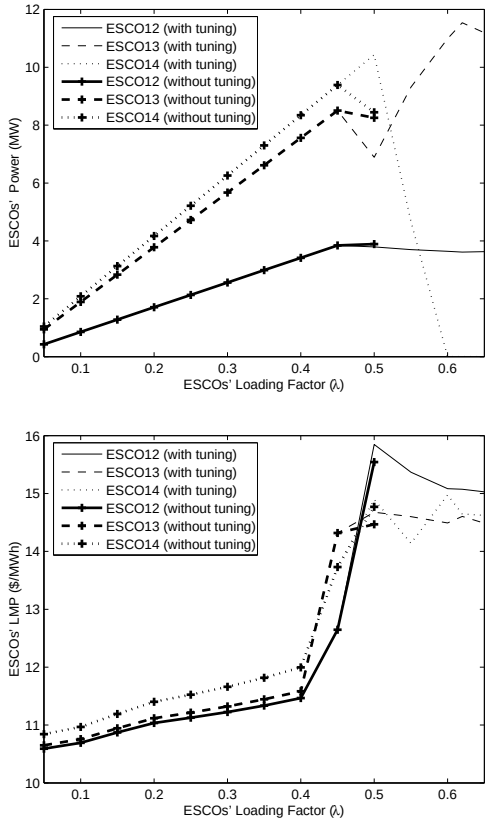

Fig. 11. Some ESCOs' power and LMPs with respect to loading factor for system with PSS.

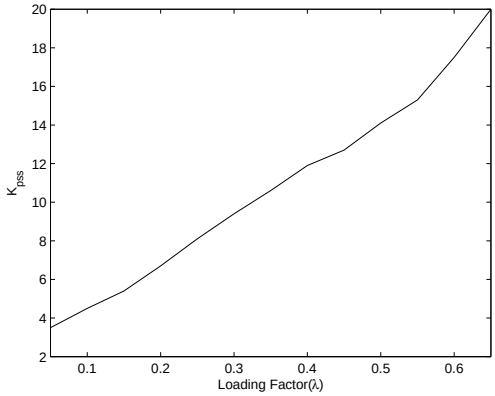

Fig. 12. The optimal value of PSS gain with respect to loading factor.

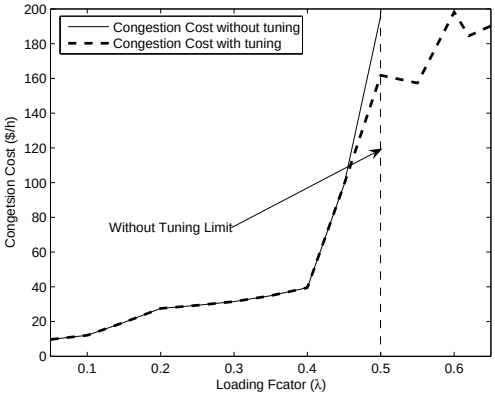

Fig. 13. Price of PSS tuning.

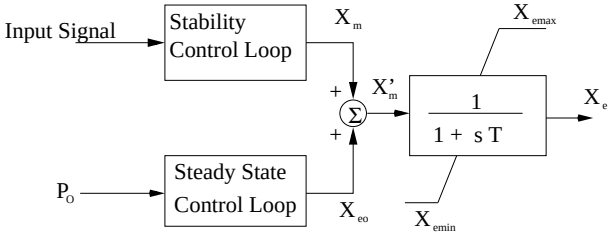

Fig. 14. TCSC model for stability studies.

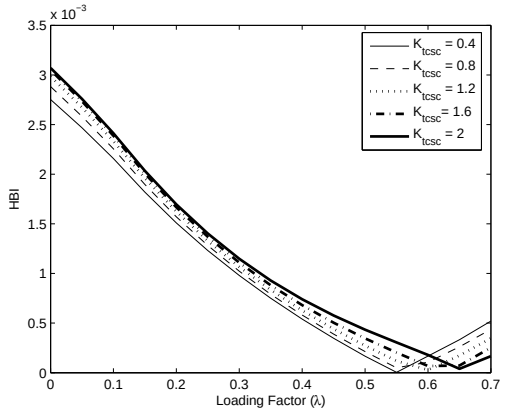

Fig. 15. Effect of the TCSC gain on the HBI.

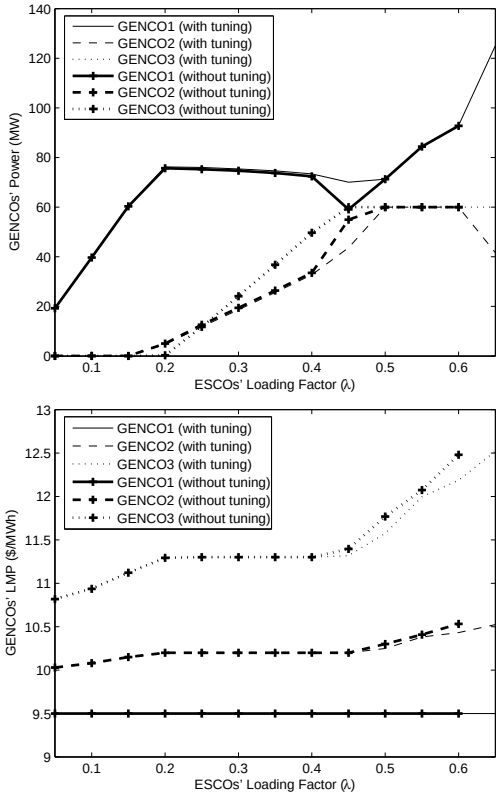

Fig. 16. GENCOs' supplied power and LMPs with respect to loading factor for the system with TCSC.

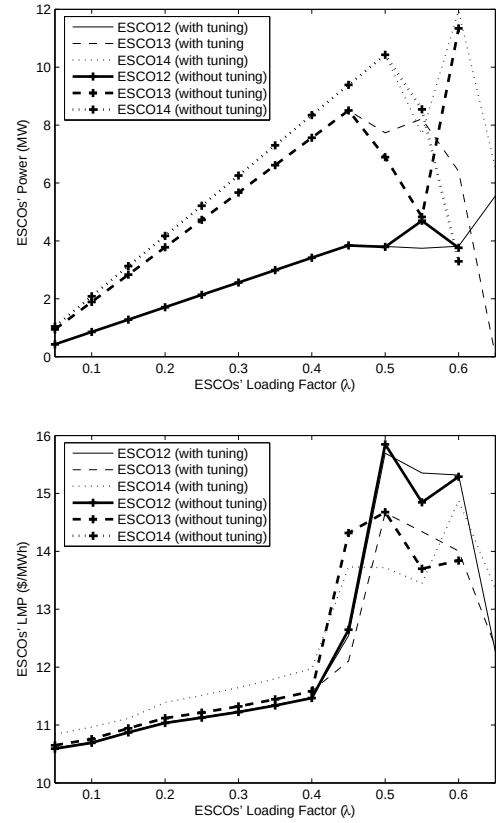

Fig. 17. Some ESCOs' power and LMPs with respect to loading factor for the system with TCSC.

B. Optimal Tuning of TCSC

The general block diagram of the TCSC model and external control structure used in this research is discussed in [32]. In this model, as depicted in Fig. 14, X_m is a modulation reactance which is determined by a stability or dynamic control loop, and X_{eo} stands for the TCSC steady state reactance or set point, whose value is provided by the steady state control loop. The sum of these two values results in X'_m, which is the net reactance order from the external control block. As the natural response of the device internal control is characterized by a delayed action, this signal is put through a first-order lag that yields the equivalent capacitive reactance X_e of the TCSC [33]. The steady state control loop may have a large time constant or be adjusted manually; hence, for large-disturbance transients X_{eo} is assumed here to be constant. The general structure of the stability controller is discussed in [32], and it consists of a washout filter with a constant gain K_{TCSC}, a dynamic compensator, and a limiter. The washout filter is used to avoid a controller response to the dc offset of the input signal. The dynamic compensator consists of two (or more) lead-lag blocks to provide the necessary phase-lead characteristics. Finally, the limiter is used to improve controller response to large deviations in the input signal.

Figure 15 shows the effect of the TCSC gain K_{TCSC} on the HBI as the ESCOs' demand power is increased from its nominal value according to (21) with $P_d = \lambda P_{L_o}$. The HBI index is calculated assuming once more that the total demand is shared between GENCO1, GENCO2 and GENCO3 in proportion to their inertias, i.e. OPF techniques are not applied in this case to determine optimal schedules. Observe the effect of changes in K_{TCSC} on the system stability, as expected; in general, as this gain is increased, the system becomes more stable, with the loadability margin increasing.

The power outputs and LMPs of all GENCOs are shown in Fig. 16 for SSC-OPF problem (7), with and without optimal tuning, with the inclusion of the TCSC controller. The TCSC gain for the SSC-OPF problem with fixed K_{TCSC} is set to 1.3, which corresponds to a 2% damping ratio at the original Hopf bifurcation point $\lambda = 0.45$ p.u. Notice that the powers and LMPs of GENCOs behave similarly as observed for the PSS example as the loading factor increases. Similar results are obtained for the ESCOs' powers and LMPs, as depicted in Fig. 17. Figure 18 depicts the optimal TCSC gain as the demand increases; as expected, the optimal TCSC gain increases more rapidly when the loading factor gets closer to the original Hopf bifurcation point ($\lambda \approx 0.45$).

As in the case of the PSS controller, Fig. 19 shows the difference between the congestion costs obtained with and without the optimal tuning technique. Notice that the difference in congestion cost can be significant without the optimal tuning technique, especially near the Hopf bifurcation point ($\lambda \approx 0.6$). These results highlight again the need for optimally tuning the controllers as the ESCOs' demand changes.

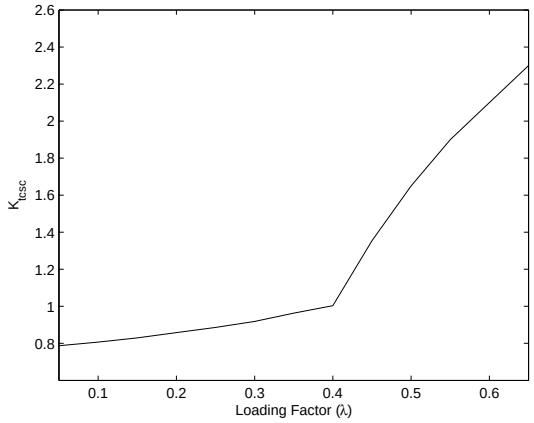

Fig. 18. The optimal value of TCSC gain with respect to loading factor.

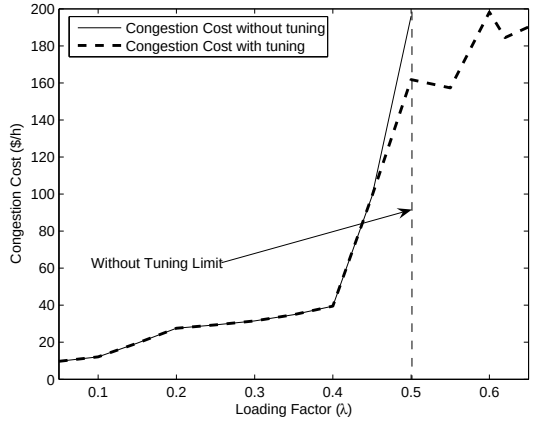

Fig. 19. Price of TCSC tuning.

V. Conclusions

An optimal tuning technique for oscillation damping controllers is discussed and tested on a benchmark test system. The proposed technique is based on a SSC-OPF which includes a stability constraint to predict oscillatory and voltage instabilities in the system. The SSC-OPF is compared to a standard OPF auction, and the results show that the SSC-OPF offers better market and system operating conditions based on a more accurate representation of system security. The SSC-OPF technique is then applied to the optimal tuning of a PSS and a TCSC, and the results show that by properly tuning these controllers, more secure operating conditions (e.g. increased loadability margins) and better market signals (e.g. lower prices) are obtained.

The proposed technique is computationally expensive, and hence more work to improve the techniques to solve the SSC-OPF model is needed to make it more useful fro practical applications. The authors are currently working on the development of new solution methodologies based on matrix semi-definiteness concepts associated with the implicit constraint of the proposed optimization model.

References

[1] A. Tiranuchit and R. J. Thomas, "A Posturing Strategy Against Voltage Instabilities in Electric Power System," *IEEE Trans. on Power Systems*, vol. 3, no. 1, pp. 87–93, February 1988.

[2] P. A. Lof, T. Smed, G. Andersson, and D. J. Hill, "Fast Calculation of a Voltage Stability Index," *IEEE Trans. on Power Systems*, vol. 7, no. 1, pp. 54–64, February 1992.

[3] C. A. Cañizares, W. Rosehart, A. Berizzi, and C. Bovo, "Comparison of Voltage Security Constrained Optimal Power Flow Techniques," in *Proc. IEEE-PES Summer Meeting*, Vancouver, BC, Canada, July 2001.
[4] F. Milano, C. A. Cañizares, and M. Invernizzi, "Multi-objective Optimization for Pricing System Security in Electricity Market," *IEEE Trans. on Power Systems*, vol. 18, no. 2, pp. 596–604, May 2003.
[5] C. A. Cañizares, N. Mithulananthan, F. Milano, and J. Reeve, "Linear Performance Indices to Predict Oscillatory Stability Problems in Power System," *IEEE Trans. on Power System*, vol. 19, no. 2, pp. 1023–1031, May 2004.
[6] D. Gan, R. J. Thomas, and R. D. Zimmerman, "Stability-Constrained Optimal Power Flow," *IEEE Trans. on Power Systems*, vol. 15, no. 2, pp. 535–540, May 2000.
[7] S. K. M. Kodsi and C. A. Cañizares, "Stability-Constrained Optimal Power Flow and Its Application to Pricing Power System Stabilizers," in *Proc. 37th North American Power Symposium*, Ames, Iowa, USA, October 2005.
[8] H. F. Wang, "Selection of Operating Conditions for the Co-ordinated Setting of Robust Fixed-Parameter Stabilizers," *IEE Proc.- Generation, Transmission and Distribution*, vol. 145, no. 2, pp. 111–116, March 1998.
[9] I. Kamwa, G. Trudel, and D. Lefebvre, "Optimization-Based Tuning and Coordination Flexible Damping Controllers for Bulk Power Systems," in *Proc. 1999 IEEE International Conference on Control Applications*, Kohala Cost-Island of Hawaii, Hawaii, August 1999.
[10] X. Lei, E. N. Lerch, and D. Povh, "Optimization and Coordination of Damping Controls for Improving System Dynamic Performance," *IEEE Trans. on Power Systems*, vol. 16, no. 3, pp. 473–480, August 2001.
[11] M. A. Abido, "Robust Design of Multimachine Power System Stabilizers Using Simulated Annealing," *IEEE Trans. on Power Systems*, vol. 15, no. 3, pp. 297–304, September 2000.
[12] Y. L. Abdel-Magid, M. A. Abido, and A. H. Mantawy, "Robust Tuning of Power System Stabilizers in Multimachine Power Systems," *IEEE Trans. on Power Systems*, vol. 15, no. 2, pp. 735–740, May 2000.
[13] Y. L. Abdel-Magid and M. A. Abido, "Optimal Multiobjective Design of Robust Power System Stabilizers Using Genetic Algorithms," *IEEE Trans. on Power Systems*, vol. 18, no. 3, pp. 1125–1132, August 2003.
[14] A. Andreoiu, K. Bhattacharya, and C. Cañizares, "Pricing Power System Stabilisers using Game Theory," *IEE Proc.-Generation, Transmission and Distribution*, vol. 152, no. 6, pp. 780–786, November 2005.
[15] I. El-Samahy, K. Bhattacharya, and C. A. Cañizares, "A Unified Framework for Reactive Power Management in Deregulated Electricity Markets," in *Proc. Power System Conference and Exposition (PSCE)*, Atlanta, Georgia, 2006, p. 7 pages.
[16] M. A. B. Zammit, D. J. Hill, and R. J. Kaye, "Designing Ancillary Services Markets for Power System Security," *IEEE Trans. Circuits and Systems*, vol. 15, no. 2, pp. 675–680, May 2000.
[17] K. Xie, Y. H. Song, J. Stonham, E. Yu, and G. Liu, "Decomposition Model and Interior Point Methods for Optimal Spot Pricing of Electricity in Deregulation Environments," *IEEE Trans. on Power System*, vol. 15, no. 1, pp. 39–50, February 2000.
[18] B. S. Gisin, M. V. Obessis, and J. V. Mitsche, "Practical Methods for Transfer Limit Analysis in the Power Industry Deregulated Environment," in *Proc. PICA IEEE International Conference*, 2000, pp. 261–266.
[19] IEEE/CIGRE Joint Task Force on Stability Terms and Definitions, "Definitions and Classification of Power System Stability," *IEEE Trans. on Power Systems*, vol. 19, no. 3, pp. 1387–1401, August 2004.
[20] C. A. Cañizares, editor, "Voltage Stability Assessment: Concepts, Practices and Tools," IEEE/PES Power System Stability Subcommittee Special Publication, SP101PSS, Tech. Rep., August 2002.
[21] N. Mithulananthan, C. A. Cañizares, J. Reeve, and G. J. Rogers, "Comparison of PSS, SVC and STATCOM Controllers for Damping Power System Oscillations," *IEEE Trans. on Power System*, vol. 18, no. 2, pp. 786–792, May 2003.
[22] P. Sauer and M. Pai, *Power System Dynamics and Stability*. Prentice Hall, 1998.
[23] C. A. Cañizares, N. Mithulananthan, A. Berizzi, and J. Reeve, "On the Linear Profile of Indices for the Prediction of Saddle-node and Limit-induced Bifurcation Points in Power Systems," *IEEE Transactions on Circuits and Systems-I*, vol. 50, no. 12, pp. 1588–1595, December 2003.
[24] G. L. Torres and V. H. Quintana, "An Interior Point Method for Nonlinear Optimal Power Flow Using Voltage Rectangular Coordinates," *IEEE Trans. on Power System*, vol. 13, no. 4, pp. 1211–1218, November 1998.
[25] V. H. Quintana and G. L. Torres, "Introduction to Interior-Point Methods," *IEEE PICA*, May 1999, santa Clara,CA.
[26] E. Castillo, A. J. Conejo, P. Pedregal, R. Garcia, and N. Alguacil, *Building and Solving Mathematical Programming Models in Engineering and Science*. John Willey & Sons, Inc., 2002.
[27] V. Vittal, Chairman, "Transient Stability Test System for Direct Stability Methods," *IEEE Trans. Power Systems*, vol. 7, no. 1, pp. 37–42, February 1992.
[28] S. K. M. Kodsi and C. A. Cañizares, "Modeling and Simulation of IEEE 14-bus System with FACTS Controllers," University of Waterloo, Waterloo, Ontario, Canada., Tech. Rep. 2003-3, March 2003.
[29] N. Mithulananthan, "Hopf Bifurcation Control and Indices for Power System with Interacting Generator and FACTS Controllers," Ph.D. dissertation, University of Waterloo, Waterloo, ON, Canada, 2002. Available at http://www.power.uwaterloo.ca.
[30] D. H. Wilson, K. Hay, and J. Toal, "Probability of Oscillatory Instability and its Implications," in *Proc. Bulk Power System Dynamic and Control VI*, Cortina d'Ampezzo, Italy, August 2004.
[31] P. M. Anderson and A. A. Fouad, *Power System Control and Stability*. AMES, IOWA, U.S.A.: The Iowa State University Press, 1977.
[32] A. D. D. Rosso, C. A. Cañizares, and V. M. Doña, "A Study of TCSC Controller Design for Power System Stability Improvement," *IEEE Trans. on Power Systems*, vol. 18, no. 4, pp. 1487–1496, November 2004.
[33] J. Paserba, N. M. amd E. larsen, and R. Piwko, "A Thyristor Series Controlled Compensation Model for Power System Stability Analysis," *IEEE Trans. on Power Systems*, vol. 10, no. 4, pp. 1471–1478, November 1995.

Sameh K. M. Kodsi (SM'02) received the B.SC. (1994) and M. Sc. (2000) degrees in Electrical Engineering degrees from Ain Shams University, Cairo, Egypt. In 2005, he received his Ph.D. in Electrical Engineering at the University of Waterloo, Ontario, Canada, and is currently a Management Consultant in Power at AMEC Americas in Oakville, Ontario.

Claudio A. Cañizares (SM'86, M'91, SM'00, F'07) received in April 1984 the Electrical Engineer diploma from the Escuela Politécnica Nacional (EPN), Quito-Ecuador, where he held different teaching and administrative positions from 1983 to 1993. His MS (1988) and PhD (1991) degrees in Electrical Engineering are from the University of Wisconsin-Madison. Dr. Cañizares has held various academic and administrative positions at the E&CE Department of the University of Waterloo since 1993 and is currently a Full Professor. His research activities concentrate on the study of stability, modeling, simulation, control and computational issues in power systems within the context of electricity markets.